Response of urban heat island to future urban expansion over the Beijing–Tianjin–Hebei metropolitan area

Abstract: Urban expansion plays a dominant role in the urban heat island (UHI) formation and is thus the essence and fundamental characteristic of the urban fabric. In this study, the responses of UHI to the urban expansion in the past decades were simulated using the coupled weather research forecast/urban canopy model (WRF/UCM) system from the 1980s to 2005 and in the future in 2050 embedded with the fine spatial resolution land use/land cover (LULC) datasets over the Beijing–Tianjin–Hebei (BTH) metropolitan area. With the urban expansion, the validations suggest that the designed models in this research can well simulate the generation and development of UHI. Due to urban expansion, the minimum temperature would rise by about 5 K in the newly developed areas. The temperature over the old urban areas would also be increased (<1 K) because of the surrounding newly developed urban areas. The footprint of urban growth, in particular the minimum temperature, is clearly captured in the three scenarios by almost all the variables. These results are quite interesting, and it indicates a more uncomfortable urban environment in the future, especially at night, when the temperature changes are larger due to urban expansion.

1. Introduction

There has been a surge of urban expansion in China, with urban areas increasing by over 20% from 1980 to 2005 (Liu and Tian 2010). In view of high economic growth and population density in China, there is an upward trend seen in urbanization. Urban climate phenomenon (UHI) has been the result of the urbanization process accompanied by the conversion from rural to urban. Statistical models, in particular correlation and regression, have been employed widely to determine the effect of urbanization on surface UHI (SUHI). Land surface temperature (LST) derived from thermal infrared (TIR) remote sensing images correlated with LULC change, built-up areas, and vegetation in cities (Bounoua et al. 2009; Chen et al. 2006; Connors et al. 2013; Guo et al. 2012; He et al. 2007; Weng et al. 2004, 2006; Zhang et al. 2013). Although statistical models are useful to describe the patterns and explore the associated factors of the UHI, they cannot reveal the generation and development of UHI (Voogt and Oke 2003). In addition, remote sensing images measure only the surface skin temperature, while the near-surface air temperature correlates more to human comfort. Although these two types of temperatures are closely related, they are actually different (Gallo et al. 2011). A series of sensitivity experiments are necessary to get a deeper insight into the UHI and the effects of urban expansion on UHI from a modeling perspective.

Recently, the weather research forecast (WRF) numerical modeling system (Skamarock et al. 2005) has attracted much attention. This meso-scale numerical

42   modeling system is designed for atmospheric research and operational forecasting.

43   Some large cities and urban agglomerations, such as Tokyo (Kusaka and Kimura

44   2004), Taipei (Lin et al. 2008; Lin et al. 2010), Nanjing (Yang et al. 2012), and

45   Beijing (Miao et al. 2009; Zhang et al. 2009), as well as Yangtze River Delta (Zhang

46   et al. 2010), the BTH metropolitan area (Wang et al. 2013a, b), and Pearl River

47   Delta (Cheng and Chan 2012; Wang et al. 2009), have witnessed the simulation of

48   the variation in UHI using this modeling system. The capability of the WRF

49   modeling system has been highlighted to explore the impact of LULC change on

50   UHI at the local or regional scales. However, when simulating the effect of urban

51   expansion on UHI (Wang et al. 2012), most studies focused only on the ideal

52   experiments (e.g., replacing urban areas by cropland), which is insufficient to

53   characterize the real urbanization process. The default LULC data from the United

54   States Geological Survey (USGS) or Moderate Resolution Imaging

55   Spectroradiometer (MODIS) products in the WRF modeling system may lead to bias

56   because of its coarse spatial resolution (Lin et al. 2010). To simulate the effect of

57   urban expansion on the UHI over the BTH metropolitan area, in this study, the

58   coupled WRF/UCM modeling system embedded with three periods of fine spatial

59   resolution LULC data were used. Part of this study included scenarios of future

60   urbanization simulated using LULC predicted by a land conversion model (Huang et

61   al 2009).

62   **2. Study area and data**

63 2.1 Study area

64 The BTH metropolitan area is situated in the North China Plain. Since being branded

65 as an economic center of northern China, this area has undergone dramatic economic

66 growth and massive urbanization from the time of the reform process in late 1978.

67 The total residential population over this region has doubled from 1984 to 2008

68 (China City Statistical Yearbook, 2009). Likewise, the built-up area expanded to a

69 large extent taking up areas which were previously agricultural zones. This study

70 takes the metropolis area as the study area, including Beijing, Tianjin, and most parts

71 of Hebei province, which is indicated by the inner rectangle in Fig. 1. The two red

72 rectangles represent the two domains in WRF model design, which is explained in

73 Section 3.
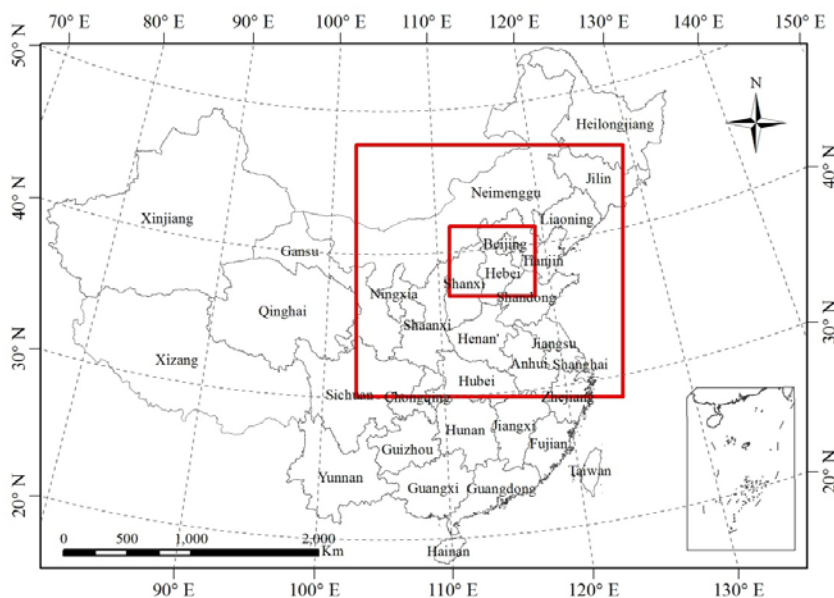
74

75   Fig.1. Study area and the two nested domains in WRF simulations.

76   2.2 Data

77   2.2.1   Land use and land cover data

78   LULC datasets in the 1980s and 2005 covering the BTH metropolis area were

79   obtained from *"Data Sharing Infrastructure of Earth System Science, the Chinese*

80   *Academy   of   Sciences   (DSIESS,CAS)"*

81   (http://www.geodata.cn/Portal/metadata/viewMetadata.jsp?id=100101-11860).   They

82   have a high accuracy of 80–90% when compared to extensive field surveys (*DSIESS,*

83   *CAS*). These datasets have a fine spatial resolution (100 m by l00 m) and are suitable

84   for characterizing urban growth between the 1980s and 2005.

85   To embed the fine spatial resolution LULC data into the WRF modeling system, they

86   were resampled to dimensions of 1×1 km using the "majority" resampling technique.

87   They were then reclassified according to the default USGS-24 categories and

88   re-projected to WGS-84. The final LULC maps are shown in Fig. 2a, b. The LULC in

89   2050 (Fig. 2c) was predicted using the statistical land conversion model by Huang et

90   al. (2009), which is introduced in Section 3.1. The three periods of LULC data in the

91   1980s, 2005, and 2050 were used to characterize the real urbanization process in the

92   past decades and the future possible pattern of urbanization. All of them were finally

93   embedded into the coupled WRF/UCM modeling system.
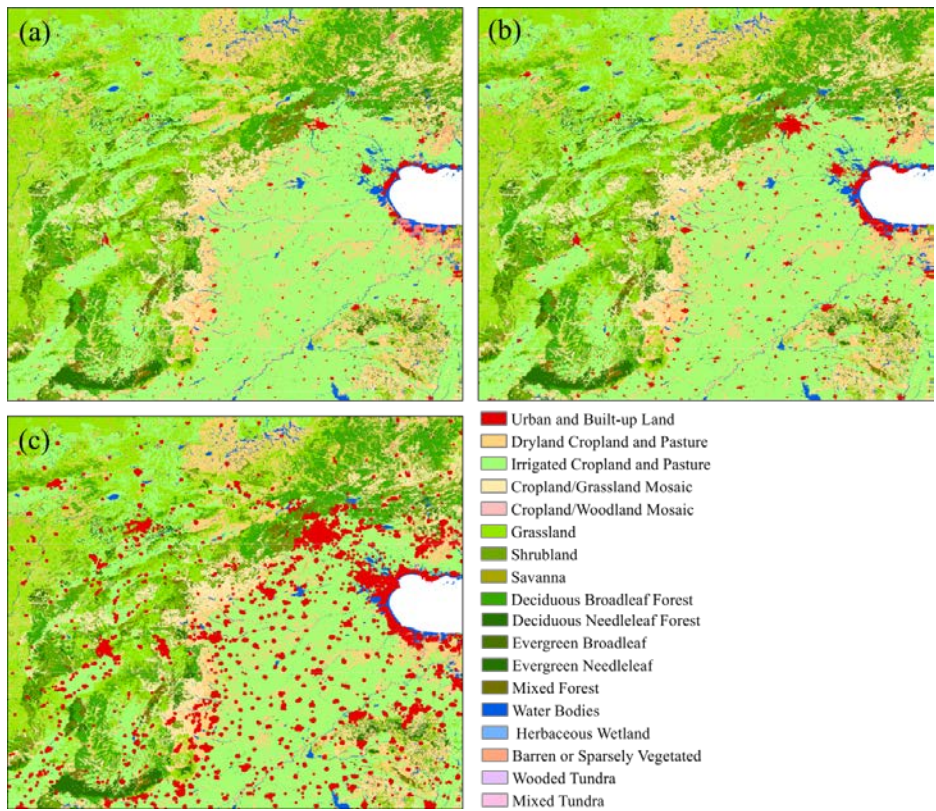
Fig.2. Land use/land cover types in (a) the 1980s, (b) 2005, (c) 2050 in the study area

2.2.2 Reanalysis data

Reanalysis data used in this research were obtained from the "*National Centers for Environmental Prediction/*Global Forecast System *(NCEP/GFS)*" *(http://www.nco.ncep.noaa.gov/pmb/products/gfs/)*. The datasets provide both the initial and the boundary conditions on 1° by 1° grids at every 6 h continuously (including 00:00, 06:00, 12:00, 18:00) for the WRF simulation.

2.2.3 Meteorological data

To validate the accuracy of the designed model in this study, the air temperature

104   data were obtained from the "*China Meteorological Data Sharing System*"

105   (http://cdc.cma.gov.cn/home.do). Nineteen meteorological stations distributed in the

106   study areas were used, which are listed in Section 3.

107   3.   Methodology

108   3.1 Statistical land conversion model

109   In this study, a statistical land conversion model developed by Huang et al. (2009)

110   was used to simulate urban–rural LULC conversion. This model was proposed by

111   establishing the logistical regression relationship between the land change (e.g., zero

112   was considered as "no change", 1 was considered as "change") and the explanatory

113   factors. In this study, the urban–rural conversion in the year 2050 was forecasted. To

114   produce the dependent urban–rural map in the 1980s and 2005, the urban built-up

115   areas were reclassified as the "urban" category, the seas and deserts were

116   reclassified as "others", and all the other types were reclassified as the "rural"

117   category. Five explanatory factors, including percentage of urban area, Euclidian

118   distance to urban area, Euclidian distance to roads, population density, and slope,

119   were employed to predict land conversion from rural to urban areas. The datasets,

120   which were used to derive the explanatory factors, were obtained from the DSIESS,

121   CAS, including road, population density, and digital elevation data.

122   3.2 WRF/UCM simulation

123   3.2.1   Parameterization schemes

124   The UCM, together with the newest 3.5.1 version of the WRF modeling system, was

125   employed in this study. With the spatial resolution adjusted at 20 km for the outer

126   domain and 4 km for the inner domain, respectively, two levels in a nested grid were

127   used (Fig. 1). The inner nested urban domain, D02, was centered over the BTH

128   metropolitan area. The outer domain, D01, covering most of northern China,

129   presented the boundary conditions for the inner domain. The geophysical coordinate

130   system adopted in this study was the Lambert projection.

131   In the case of the input parameters required by the WRF modeling system, the initial

132   boundary conditions were supplied by the NCEP/GFS 6-hourly reanalysis data (see

133   *Section* 2.2.2, *Reanalysis data*). The terrestrial, geographical input data had a spatial

134   resolution of 30". The default USGS LULC data were replaced by the fine spatial

135   resolution LULC data (see *Section* 2.2.1, *Land use and land cover data*). The main

136   physical parameterization schemes adopted in this study are shown in Table 1.

137   The simple single-layer UCM was used to take the geometry of urban areas into

138   account in the wind shear and surface energy budget calculations (Chen et al. 2011;

139   Chen et al. 2004; Kusaka et al. 2001). As it is difficult to obtain the detailed urban

140   structures for all cities over the study area, the uniform urban canopy parameters and

141   the default hourly diurnal profile of anthropogenic heat in a typical urban area set in

142   the UCM were employed in this study (Table 2).

143   Table 1 Physical parameterization schemes used in this study.

Physical processes	Parameterization scheme
Microphysics scheme	WSM 3-class simple ice scheme
Cumulus scheme	Grell–Devenyi ensemble scheme
Surface layer	Monin–Obukhov scheme
Land surface process	Noah land surface model
Planetary boundary layer process	YSU scheme
Long-wave radiation	RRTM scheme
Short-wave radiation	Dudhia scheme

144   Table 2 Default parameters in the coupled WRF/UCM modeling system (Sources:

145   Wang et al. 2012).

Description	Value	Units
Building height	7.5	m
Road width	9.4	m
Fraction of the urban landscape occupied by artificial materials	0.9	
Surface emissivity of roof/building all/road	0.9	
Surface albedo of roof/building all/road	0.2	
Anthropogenic heat	50	Wm^{-2}
Hourly diurnal profile for anthropogenic heat (starting at 01 h local time)	0.16, 0.13, 0.08, 0.07, 0.08, 0.26, 0.67, 0.99, 0.89 0.79, 0.74, 0.73, 0.75, 0.76, 0.82, 0.90, 1.00, 0.95, 0.68, 0.61, 0.53, 0.35, 0.21, 0.18	

146   3.2.2   Experiments design

147   During the study period and the two-level nested spatial domains (Chen et al. 2011,

148   Skamarock et al. 2005), the global and regional warming effects were embedded in all

149   the simulation scenarios by the input reanalysis data. This study also included

150   sensitivity experiments by changing the underlying LULC data to explore the impacts

151   of urban expansion on the UHI. In addition, the BTH metropolitan region has a

152   subhumid warm temperate continental monsoon climate with a cold and windy winter,

9

153 a hot and humid summer, and transitional periods in spring and autumn (Qiao et al.

154 2013). Likewise, the distinct seasonal variations in the UHI have also been described,

155 with the UHI reaching its peak intensity in summer, much lesser in spring and autumn,

156 and negative in winter (Yang et al. 2010, Liu et al. 2014; Wang et al. 2007). As we

157 intended to explore the effect of urbanization on the UHI, given the huge computer

158 resources and time–cost when running the WRF experiments, we picked the winter

159 and summer periods for the study. In all, three scenarios were designed in this study,

160 including the 1980s, 2005, and 2050. Simulated experiments were conducted during

161 January and July to present the winter and summer periods, respectively, comparing

162 the seasonal variations in UHI. Specifically, six experiments were carried out. Each

163 case was started at local time 00:00, with the first 2 days being allocated for model

164 spin-up to minimize the effect of initial conditions. To represent current urban

165 conditions, the LULC data in 2005 were used, and the two cases in 2005 were used as

166 control experiments to validate the performance of the designed models. The

167 experiments in the 1980s and 2050 were used as the compared experiments presenting

168 the early and future urbanization simulations, respectively.

169 4. **Results and discussion**

170 4.1 Validation of the control experiments

171 The performance of the two control experiments in January and July in 2005 was

172 tested by comparing the simulated 2-m temperature and 10-m wind speed with the

173 observed air temperature and wind speed from 19 meteorological stations in the

10

study area (Fig. 3). A simulated average of 2-m temperature and 10-m wind speed

was achieved within the 3 × 3 pixels surrounding each meteorological station. In

January, the correlation coefficient (CC) between the observed and simulated values

was significant at the 0.001 level (CC: 0.84 for the temperature and 0.86 for the

wind speed). Although a slightly larger absolute error existed for some dates, such

as July 14, the overall trend of simulated 2-m temperature was consistent with the

observed air temperatures from the meteorological stations in July. The CC between

the observed and simulated values (CC: 0.37) was significant at the 0.05 level. The

simulated wind speed in July was not well matched with the observed values (CC:

0.1), the reasons for which will be explained later.
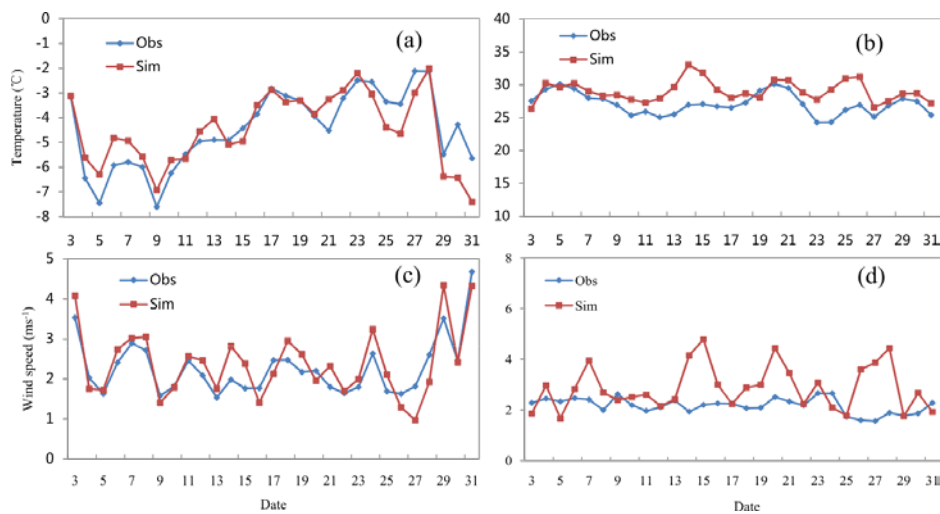
Fig.3. Comparison of values between observed (Obs) air temperature and simulated

(Sim) 2-m temperature, and between observed wind speed and simulated 10-m wind

speed averaged spatially across 19 meteorological stations. Left: January; Right:

July.

The monthly averaged simulated 2-m temperature was also compared with the

11

190   monthly average observed air temperature for each station (Table 3). In January,

191   most of the root mean square errors (RMSE) were below 1°C. The absolute errors

192   for most of the stations were within 2°C except in Weixian, Bohai A, Chengde, and

193   Zhangjiakou. In July, the RMSE was around 1.5°C for most of the stations, while

194   both the absolute errors varied between the stations, with the largest vales (3.59 °C)

195   in Beijing station and the smallest value (−0.13°C) in Bohai A station.

196   Table 3. Comparison between observed air temperature and simulated 2-m

197   temperature for each meteorological station (units: °C).

StationID	Station Name	January				July			
		Obs	Sim	RMSE	AE	Obs	Sim	RMSE	AE
54511	Beijing	−2.58	−3.45	0.78	−0.87	27.72	31.31	1.59	3.59
54416	Miyun	−5.77	−4.42	0.98	1.35	26.50	28.84	1.28	2.33
54705	Nangong	−3.25	−3.06	0.36	0.19	27.73	31.10	1.54	3.36
54624	Huanghua	−2.68	−3.92	0.93	−1.24	28.21	30.40	1.24	2.19
54618	Botou	−3.41	−3.89	0.59	−0.48	28.21	31.25	1.47	3.04
54606	Raoyang	−4.50	−4.28	0.39	0.21	27.62	30.98	1.54	3.36
54602	Baoding	−2.81	−4.08	0.95	−1.27	28.47	31.84	1.54	3.36
54534	Tangshan	−3.40	−4.41	0.85	−1.01	27.27	28.44	0.91	1.17
54518	Langfang	−3.48	−4.91	1.01	−1.43	27.77	30.83	1.47	3.06
54429	Zunhua	−4.84	−4.71	0.31	0.13	26.54	27.88	0.97	1.34
54423	Chengde	−9.80	−7.69	1.22	2.11	23.91	24.54	0.67	0.63
54405	Huailai	−6.89	−7.18	0.45	−0.29	26.00	27.06	0.87	1.06
54401	Zhangjiakou	−8.38	−11.02	1.37	−2.64	24.90	25.27	0.51	0.37
53798	Xingtai	−1.19	−1.49	0.46	−0.30	28.65	30.84	1.24	2.19
53698	Shijiazhuang	−2.08	−1.79	0.45	0.29	28.64	30.99	1.29	2.34
53593	Weixian	−12.49	−10.10	1.30	2.38	24.34	23.91	0.55	−0.43
54646	Bohai A	−1.11	1.85	1.45	2.96	26.50	26.37	0.31	−0.13
54623	Tanggu	−2.46	−2.48	0.11	−0.02	28.15	29.46	0.96	1.30
54527	Tianjin	−3.77	−4.01	0.42	−0.25	27.73	30.44	1.38	2.71

198   Obs: Observed values; Sim: simulated values; AE: Absolute error.

199   The bias between the observed and simulated values may be caused by the following

factors. First, the spatial extent of the observed values used for the validation was not perfectly consistent with that of the simulated values, which were averaged within the 3×3 pixels surrounding the metrological station, with the pixel size equal to 4×4 km. By contrast, the observed values were obtained from just one point at the metrological station. There may be a bias caused by the spatial heterogeneity. Second, the default parameters in the UCM were adopted in this study, such as the height of the building height, width of the street, and anthropogenic heat discharge. In practice, these are likely to be different from the actual conditions in the study area, which may introduce errors to the simulated values in urban areas. Third, the validation of the model performance revealed lower accuracy in summer than in winter, which was also reported by previous studies (Cheng et al. 2012). This may be caused by the frequent rainfall experienced in summer in the study area (Wu et al. 2003). Overall, as we focused on the effects of different LULC in this research, this bias can be considered as a systematic model error that will not affect the applicability of the conclusions.

4.2 Diurnal and seasonal variation in UHI at the fine spatial resolution

As there were differences in heat fluxes between rainy days and dry days (Yang et al. 2012), experiments on dry days were the ones picked and analyzed in this study. If the stations (e.g., Beijing, Miyun, Tianjin, Tanggu, Shijiazhuang, Tangshan) typically received no precipitation, the days were considered dry. In July, the 5th, 6th, 25th, 26th, and the 29th were the dry days, while in January, except 5th and 6th, all

221   the days were dry. The simulated surface skin temperatures at local times 02:00,

222   08:00, 14:00, and 20:00 in January and July 2005 are presented in Fig.4. The SUHI

223   was observed to be distinct in July, while the SUHI in January was not so obvious.

224   In the case of the SUHI in July, the nighttime SUHI at 02:00 and 20:00 was much

225   larger than the daytime SUHI at 08:00 and 14:00. The spatial pattern of 2-m

226   temperature was consistent with the surface skin temperature (figures are not shown

227   here). The air UHI (AUHI) in July was significantly larger than that in January,

228   while the nighttime AUHI in July was significantly greater than the daytime AUHI.

229
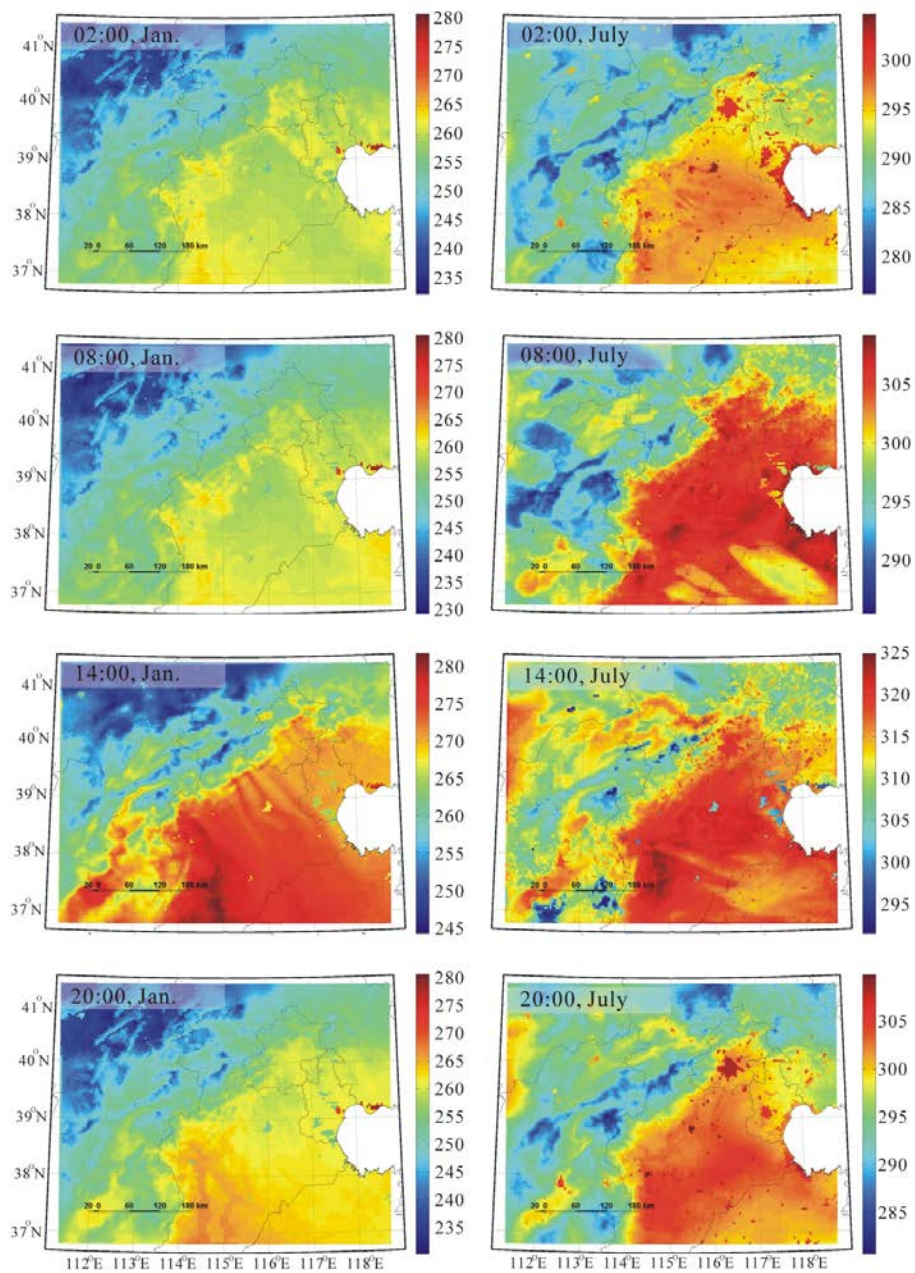
Fig.4. Surface skin temperature (TSK) at 02:00, 08:00, 14:00, and 20:00 (from top to

bottom). Left: January; Right: July.

The SUHI intensity (SUHII) and AUHI intensity (AUHII) were calculated by

subtracting the average temperature in urban areas (here urban and built-up land)

15

234 from the average temperature in rural areas (here cropland). Figure 5 shows the

235 diurnal variation of both the SUHII and AUHII in July 2005. The AUHII was lower

236 than the SUHII for the entire day. The SUHII was larger during the night and

237 reached the highest value (6 K) around 04:00. It was much smaller during the

238 daytime and had the smallest value (2 K) around 12:00. Generally, the trend of the

239 diurnal variation of AUHII was consistent with the SUHII, but with about 2 K lower

240 temperature than the SUHII during the nighttime and about 1 K lower during the

241 daytime. Overall, both the simulated 2-m AUHII and SUHII were larger during the

242 nighttime than during the daytime.
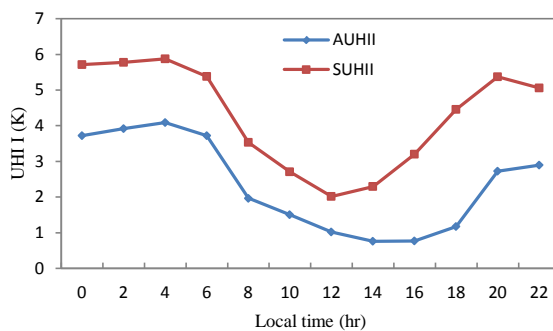
243

244 Fig.5. Diurnal variation in simulated 2-m air UHII (AUHII) and surface UHII

245 (SUHII) in July 2005.

246 In other studies (Yang et al. 2010, Liu et al. 2014; Wang et al. 2007), the greatest

247 UHI intensity in summer and the very small UHI (even the "cool" island) in winter

248 were also observed. This can be explained by differences in vegetation coverage and

249 the human heat discharge between urban and rural areas during summer and winter.

250 During summer, significant negative correlations between the vegetation and the

16

251 surface temperatures were documented, which suggests that the greater the

252 vegetation coverage, the lower the temperature (Gallo et al. 1996, Weng 2009). This

253 essentially is a result of the absorption and transpiration effect of vegetation. During

254 summer, the vegetation coverage in the urban areas was much lower in comparison

255 to rural areas in the BTH metropolitan area (Zhang et al. 2005). Then, in summer,

256 the rural areas with greater vegetation coverage would have lower temperatures than

257 urban areas. Besides, the large human heat released by air conditioning in buildings,

258 industrial production, and combustion engines, etc., in the urban areas can also

259 increase temperatures in the urban areas in comparison to rural areas. In winter, the

260 vegetation coverage in both the rural and urban areas in the BTH metropolitan

261 region is low. Large areas of bare soil exist in the rural areas, which can store a large

262 amount of heat with higher temperatures. In contrast, cold sources in such cold

263 building surfaces in urban areas may make urban areas cool in winter. Besides, the

264 BTH metropolitan area is located in the northern hemisphere. The low solar altitude

265 creates shadows from buildings in urban areas in winter, which also lead to less

266 shortwave radiation in the shadows and lower temperatures in urban areas.

267 4.3 Effect of urban expansion on the UHI

268 To explore the effect of urban expansion on the UHI (Fig. 6), the daily mean,

269 maximum, and minimum surface skin temperatures, for dry days, in July, were

270 compared between the 1980s, 2005, and 2050. The remarkable changes of the daily

271 mean temperature, in the three periods (upper row in Fig. 6), could be captured with

17

272   the footprint of the urban expansion. The effects of LULC change on the

273   temperature were small for the maximum temperature (middle row in Fig. 6), and

274   the UHI could be hardly identified. The UHI was generally best revealed in the

275   minimum temperature maps in all three scenarios (lower row in Fig .6). The

276   footprint of the newly developed urban areas was also clearly captured by the maps.

277   Similar spatial patterns can also be observed in the 2-m air temperature maps

278   (Figures are not shown here).

279   To confirm the significant effect of urbanization on temperature, especially the

280   minimum temperature, relative frequency distribution curves were plotted

281   highlighting the temperature changes caused by urban expansion (Fig. 7). The

282   changes of mean, maximum, and minimum surface skin temperature, during three

283   scenarios, were barely discernible over the old urban areas in the 1980s (left column

284   in Fig. 7). Over the newly developed urban areas in 2005 (middle column in Fig. 7),

285   the mean, maximum, and minimum surface skin temperature in 2005 and 2050 are

286   obviously larger than those in the 1980s, with an increase of about 5 K for the mean

287   and minimum surface skin temperature and about 2 K for the maximum surface skin

288   temperature. The frequency distribution curves for the mean, maximum, and

289   minimum surface skin temperature in 2050, in comparison to the newly developed

290   urban areas in 2050 (right column in Fig. 7), were also clearly distinguishable from

291   the 1980s and 2005, with an increase of about 5 K for the mean and minimum and

292   about 2 K for the maximum surface skin temperature. A similar magnitude for the

293   effect of urban growth on the 2-m temperature was also observed.
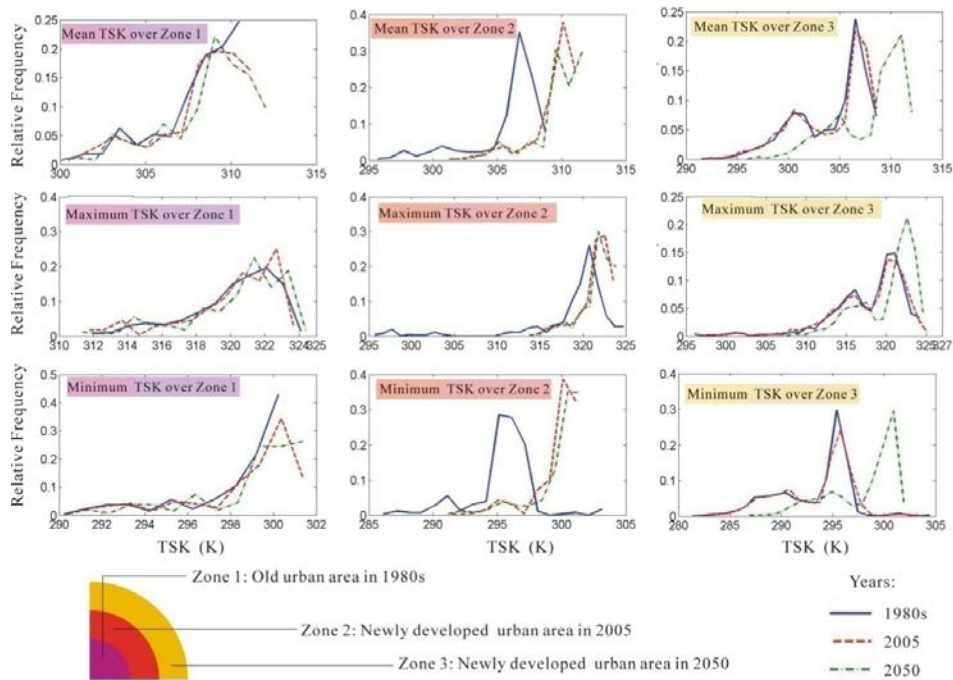
294
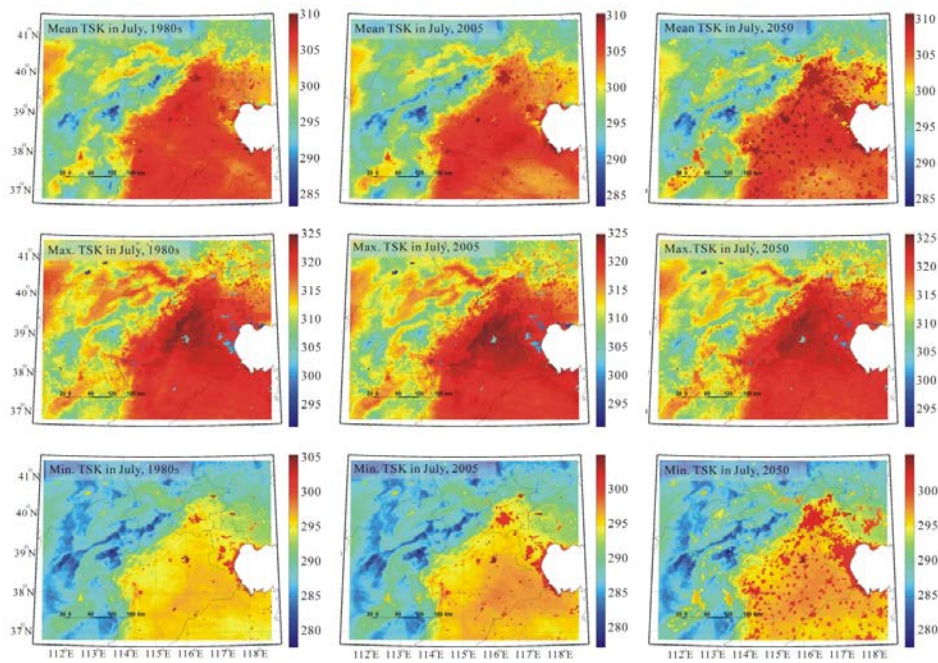
Fig.6. Surface skin temperature in the 1980s, 2005, 2050: 1) daily mean TSK (upper

row); 2) daily maximum TSK (middle row); 3) daily minimum TSK (below row) for

fine day in July in the 1980s (left column), 2005 (middle column) and 2050 (right

column).

Fig.7. Relative frequency distribution curves for daily mean (above row), maximum (middle row), and minimum (below row) surface skin temperature over newly developed urban areas in the 1980s (left column), 2005 (middle column), and 2050 (right column).

The largest increase in the minimum temperature by urban expansion also provided evidence through variation in the temperate change at the diurnal scale. Figure 8 (left panel) presents the diurnal cycles of surface skin temperature in the 1980s, 2005, and 2050 over old urban areas in the 1980s, newly developed urban area in 2005, and newly developed urban area in 2050. There was a distinct increase in surface skin temperatures over the newly developed urban areas, especially during the nighttime. For example, in the case of the newly developed urban area in 2005, the surface skin temperature in 2005 and 2050 increased by about 5 K during the nighttime and around

20

312   2 K during the daytime compared with that in the 1980s. The 2-m temperature also

313   presented a similar trend. The 2-m air temperature in 2005 and 2050 was about 3 K

314   higher during the nighttime and 0.5 K higher during the daytime than that in the 1980s.

315   The newly developed urban areas also increased the temperature over the old urban

316   areas, which can be reflected by the temperature differences between years (right

317   panel in Fig. 8). For example, over the old urban areas in the 1980s, the surface skin

318   temperature in 2005 was about 0.3 K higher than that in the 1980s during the

319   nighttime and nearly the same during the daytime; the surface skin temperature in

320   2050 was found to be approximately 0.6 K higher than in 2005 around at 22:00 and

321   about 0.2 K higher around at 8:00. In the case of the newly developed urban area in

322   2005, the surface skin temperature in 2050 was about 0.5 K higher than that in 2005.

323   The 2-m temperature over the old urban areas increased a little and became a bit

324   higher than the surface skin temperature (figures are not shown here). For example,

325   over the old urban areas in the 1980s, the 2-m temperature in 2005 was about 0.4 K

326   higher than that in the 1980s during the nighttime and about 0.1 K higher during the

327   daytime; the 2-m temperature in 2050 was about 0.8 K higher than that in 2005 at

328   around 22:00 and about 0.2 K at around 14:00; the 2-m temperature in 2050 would be

329   increased by 1 K more than the 1980s at around 22:00 and by more than 0.2 K at

330   around 14:00. It may be caused by the greater mobility of the 2-m temperature fields.

331   It is fair to conclude, in general, that the conversion of land from rural to urban area

332   could significantly increase the temperature, especially the minimum temperature at

333   night. The newly developed urban areas can also facilitate a slight increase slightly in

334   the temperatures in of the older urban areas.
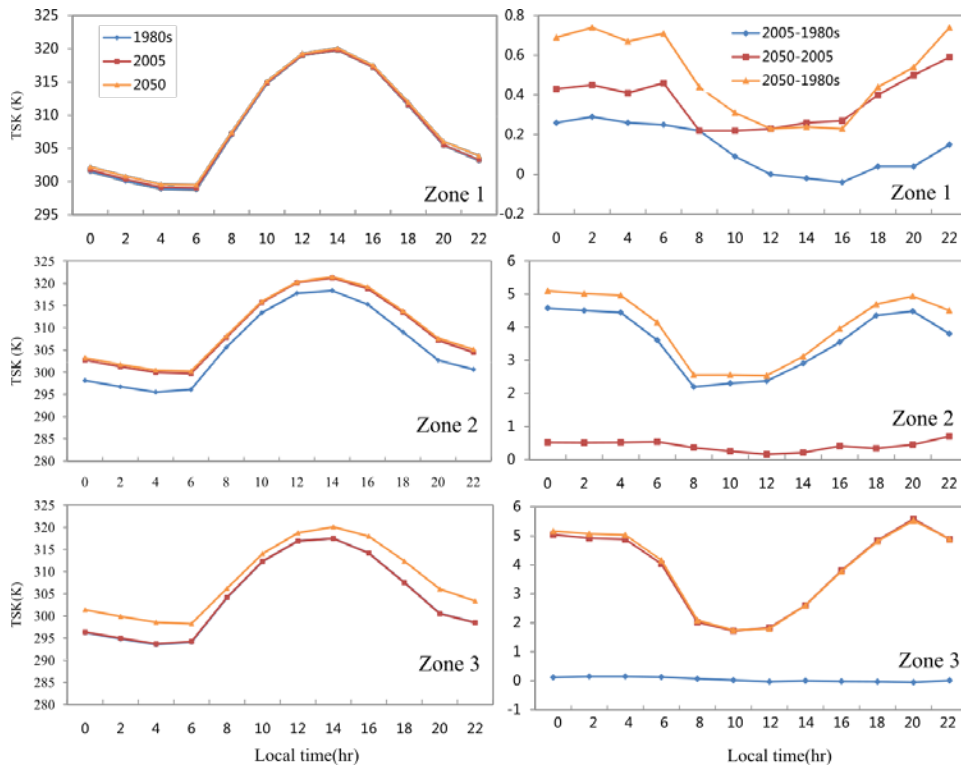
Fig.8. Averaged surface skin temperature (left) and averaged surface skin

temperature differences between years (right) over old urban areas in the 1980s

(Zone 1), newly developed urban areas in 2005 (Zone 2), and newly developed

urban areas in 2050 (Zone 3).

340   The significant effect of urban expansion on the minimum temperature, together

341   with the largest temperature increase at night, was consistent with the previously

342   observed greater UHI at night. It can be explained by the characteristics of urban

343   constructed surfaces. Impervious urban structures have a higher heat capacity that

344   can store more energy during the daytime and release the heat slowly at night. The

22

345 low sky view factor also delayed the loss of heat through multiple reflections and the

346 trapping of near-surface air in urban areas (Argüeso et al.2013). However, the

347 opposite is true over rural areas. The differences between urban and rural areas lead

348 to different heat flux characteristics, which finally contribute toward urban

349 expansion leading to increases in the minimum temperature and temperatures getting

350 warm during the night.

351 We also compared our results with the climatic simulated results from the

352 Intergovernmental Panel on Climate Change/Fifth Assessment Report (IPCC/AR5).

353 According to IPCC/AR5, the temperature changes between June and August ranged

354 from 0 to 8°C, with increasing amplitude from 2000 to 2100. During the period

355 2046 and 2065, the temperature variation would be about 4 °C, which was a little

356 different from our results. This is understandable. However, we considered only

357 urban expansion, while the simulations in the IPCC/AR5 considered both urban

358 expansion and anthropogenic heat discharge. Besides, the future pattern of

359 urbanization in this study was produced from only a statistical predictive model

360 based on five explanatory factors. Although this model has been validated in

361 previous studies (Huang et al. 2009), and can provide a possible urbanized pattern,

362 as a forecast of the real future state there is much uncertainty associated with this

363 model. However, we focused only on the BTH metropolitan area, while the

364 simulated area in the IPCC/AR5 covered Eastern Asia. It is reasonable to believe

365 that the metropolitan areas with intense human activities may have higher

366 temperature changes. It is also suggested to conduct the climatic simulation

367 regionally by accounting for human heat discharge to offer more information about

368 the effect of urbanization on the UHI.

369 4.4 Effect of urban expansion on surface heat fluxes

370 The thermal properties of the land surface can be altered by urbanization leading to

371 UHI. Diurnal variation in energy fluxes at the ground surface closely correlated to

372 diurnal variation of the UHI. This can, for example (Fig. 9), be documented by the

373 diurnal variations in the heat fluxes over the newly developed urban area in 2005.

374 During the 1980s, this zone fell under rural areas and eventually became urban area

375 in 2005 and 2050.

376 Urbanization can largely increase the sensible heat fluxes by decreasing the latent

377 heat flux (Fig. 9a-b). The urban surface had much higher sensible heat flux and

378 much lower latent heat flux than rural areas due, in part, to lower evaporation over

379 the urban surface. Although both the urban and rural areas had roughly the same

380 short-wave fluxes (Fig. 9c), the urban area gained more radiation and stored more

381 heat than rural areas (Fig.9e). Also, a higher surface temperature in urban area was

382 expected because of its large heat storage during the daytime. The active heat fluxes

383 between the underlying surface and the atmosphere also led to the much higher air

384 temperature over urban regions. The long-wave flux witnessed in urban areas was

385 much larger in comparison to rural areas (Fig. 9d) during the night. Although the

386 urban surface cools during the night, the large quantity of heat stored on the surface

387 together with heat conductivity makes the surface temperature in the urban area

24

much higher than the surface in rural areas at night. During the nighttime, the larger long-wave fluxes can heat the atmosphere in urban areas. During the nighttime, however, rural surfaces cooled rapidly. Rural regions witness heat fluxes that heat up the land underlying the surface, thereby heating the atmosphere. At night, the air temperature over urban regions was much higher than that over the rural regions. This explains why both the surface UHII and air UHII were much larger during the nighttime.
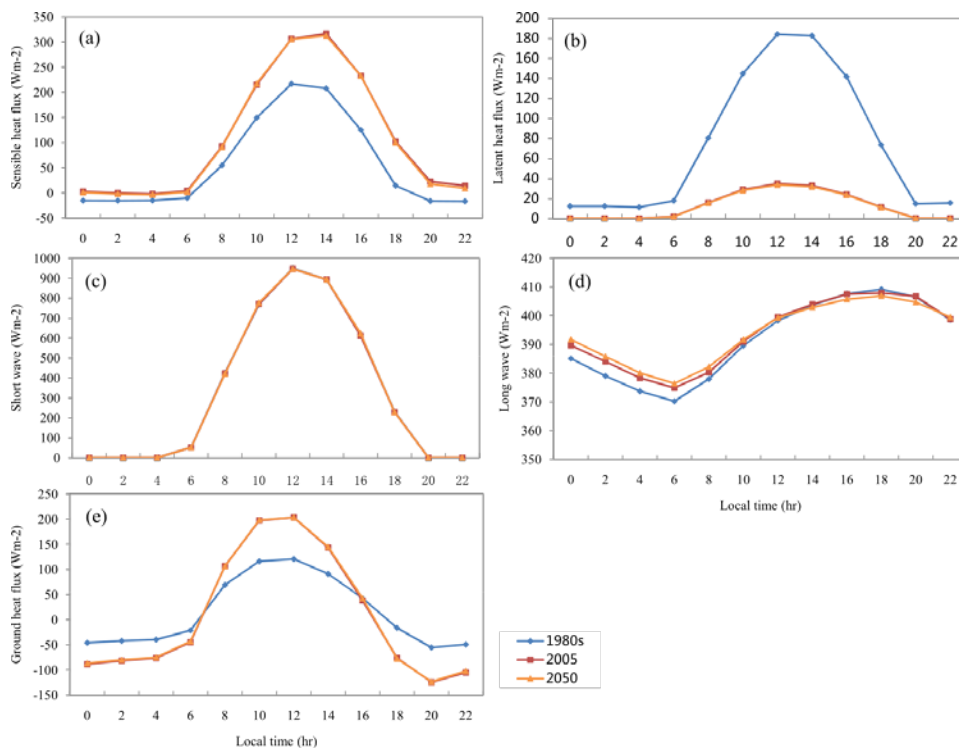
Fig. 9. Heat fluxes in July 1980s, 2005, and 2050 over newly developed urban areas in 2005.

5. **Summary**

This study was conducted using the BTH metropolitan area as the area of the study to

25

400 ascertain the effect of urban expansion on the UHI using the coupled WRF/UCM

401 modeling system. Fine spatial resolution LULC data in the 1980s and 2005 and urban

402 expansion in 2050, predicted using a statistical land conversion model, were used in

403 this study. The significant effect of urbanization on temperatures, especially the

404 minimum temperature, was quantified over both the newly developed and the old

405 urban areas, by evaluating the three scenarios in the sensitivity experiments.

406 Both the surface UHI and air UHI shared consistent seasonal and diurnal variations.

407 The UHI can be observed distinctly in July, while is not so obvious in January. The

408 UHII was larger during the nighttime and reached the largest value around 04:00 in

409 July. It was much weaker during the daytime and reached the lowest value around

410 12:00. The diurnal variation in AUHII was consistent with the SUHII, but about 2 K

411 lower than the SUHII during the nighttime and about 1 K lower during the daytime.

412 Urban expansion significantly affected the minimum temperature. The UHI can be

413 observed in all three scenarios, and the footprint of the newly developed urban areas

414 can be captured, especially in the map showing the minimum temperature. While the

415 maximum temperature increased by about 2 K, both the mean and the minimum

416 temperature would be increased by about 5 K over the newly developed urban area.

417 The temperature over the old urban area would also be increased by urban growth

418 (by <1 K). The results point to a more uncomfortable urban environment in the

419 future, with higher heat storage due to urbanization, especially during the nighttime,

420 when temperature changes are greater due to urban expansion.

References

Argüeso, D., Evans, J., Fita, L., & Bormann, K. (2013). Temperature response to future urbanization and climate change. *Climate Dynamics*, 1-17

Bounoua, L., Safia, A., Masek, J., Peters-Lidard, C., & Imhoff, M.L. (2009). Impact of urban growth on surface climate: a case study in Oran, Algeria. *Journal of Applied Meteorology and Climatology, 48*, 217-231

Chen, F., Kusaka, H., Bornstein, R., Ching, J., Grimmond, C.S.B., Grossman-Clarke, S., Loridan, T., Manning, K.W., Martilli, A., Miao, S., Sailor, D., Salamanca, F.P., Taha, H., Tewari, M., Wang, X., Wyszogrodzki, A.A., & Zhang, C. (2011). The integrated WRF/urban modelling system: development, evaluation, and applications to urban environmental problems. *International Journal of Climatology, 31*, 273-288

Chen, F., Manning, K.W., Yates, D.N., LeMone, M.A., Trier, S.B., Cuenca, R., & Niyogi, D. (2004). Development of high resolution land data assimilation system and its application to WRF. In, *Preprints, 16th Conf. on Numerical Weather Prediction, Seattle, WA, Amer. Meteor. Soc*

Chen, X.L., Zhao, H.M., Li, P.X., & Yin, Z.Y. (2006). Remote sensing image-based

444   analysis of the relationship between urban heat island and land use/cover

445   changes. *Remote Sensing of Environment, 104*, 133-146

446   Cheng, C.K.M., & Chan, J.C.L. (2012). Impacts of land use changes and synoptic

447   forcing on the seasonal climate over the Pearl River Delta of China.

448   *Atmospheric Environment, 60*, 25-36

449   Connors, J., Galletti, C., & Chow, W.L. (2013). Landscape configuration and urban

450   heat island effects: assessing the relationship between landscape characteristics

451   and land surface temperature in Phoenix, Arizona. *Landscape Ecology, 28*,

452   271-283

453   Gallo, K. P., & Tarpley, J. D. (1996). The comparison of vegetation index and

454   surface temperature composites for urban heat-island analysis. *International*

455   *Journal of Remote Sensing, 17, 3071-3076*

456   Gallo, K., Hale, R., Tarpley, D., & Yu, Y.Y. (2011). Evaluation of the relationship

457   between air and land surface temperature under clear- and cloudy-sky

458   conditions. *Journal of Applied Meteorology and Climatology, 50*, 767-775

459   Guo, Z., Wang, S.D., Cheng, M.M., & Shu, Y. (2012). Assess the effect of different

460   degrees of urbanization on land surface temperature using remote sensing

461   images. *Procedia Environmental Sciences, 13*, 935-942

462   He, J.F., Liu, J.Y., Zhuang, D.F., Zhang, W., & Liu, M.L. (2007). Assessing the

463   effect of land use/land cover change on the change of urban heat island

464   intensity. *Theoretical and Applied Climatology, 90*, 217-226

465   Huang, B., Zhang, L., & Wu, B. (2009). Spatiotemporal analysis of rural–urban land

466   conversion. *International Journal of Geographical Information Science, 23,*

467   379-398

468   Kusaka, H., & Kimura, F. (2004). Thermal effects of urban canyon structure on the

469   nocturnal heat island: numerical experiment using a meso-scale model coupled

470   with an urban canopy model. *Journal of Applied Meteorology, 43,* 1899-1910

471   Kusaka, H., Kondo, H., Kikegawa, Y., & Kimura, F. (2001). A simple single-layer

472   urban canopy model for atmospheric models: Comparison with multi-layer and

473   slab models. *Boundary-Layer Meteorology, 101,* 329-358

474   Lin, C.Y., Chen, F., Huang, J.C., Chen, W.C., Liou, Y.A., Chen, W.N., & Liu, S.-C.

475   (2008). Urban heat island effect and its impact on boundary layer development

476   and land-sea circulation over northern Taiwan. *Atmospheric Environment, 42,*

477   5635-5649

478   Lin, C.Y., Chen, W.C., Chang, P.L., & Sheng, Y.F. (2010). Impact of the urban heat

479   island effect on precipitation over a complex geographic environment in

480   northern Taiwan. *Journal of Applied Meteorology and Climatology, 50,*

481   339-353

482   Liu, M.L., & Tian, H.Q. (2010). China's land cover and land use change from 1700

483   to 2005: Estimations from high-resolution satellite data and historical archives.

484   *Global Biogeochemical Cycles, 24.*

485   Liu, S., Li, Q., &Zhu, Y. J. (2014). Study on seasonal variation of urban heat island

486   with HJ-1B satellite imagery: a case study of Beijing. *Scientia Geographical*

487   *Sinica, 34(1), 84-88*

488   Miao, S., Chen, F., LeMone, M.A., Tewari, M., Li, Q., & Wang, Y. (2009). An

489   observational and modeling study of characteristics of urban heat island and

490   boundary layer structures in Beijing. *Journal of Applied Meteorology and*

491   *Climatology, 48*, 484-501

492   Qiao, Z., Tian, G. G., &Xiao, L. (2013). Diurnal and seasonal impacts of

493   urbanization on the urban thermal environment: a case study of Beijing using

494   MODIS data. *Journal of Photogrammetry and Remote Sensing, 85, 93-101.*

495   Skamarock, W.C., Klemp, J.B., Dudhia, J., Gill, D.O., Barker, D.M., Wang, W., &

496   Powers, J.G. (2005). A description of the advanced research WRF version 2. In:

497   DTIC Document

498   Voogt, J.A., & Oke, T.R. (2003). Thermal remote sensing of urban climates. *Remote*

499   *Sensing of Environment, 86*, 370-384

500   Wang, J., Feng, J., Yan, Z., Hu, Y., & Jia, G. (2012). Nested high-resolution

501   modeling of the impact of urbanization on regional climate in three vast urban

502   agglomerations in China. *Journal of Geophysical Research: Atmospheres, 117*,

503   D21103

504   Wang,J. K., Wang K. C., &Wang, P. C. (2007). Urban heat (or cool) island over

505   Beijing from MODIS land surface temperature. *Journal of Remote Sensing,*

506   *11(3), 330-339.*

507   Wang, M., Yan, X., Liu, J., & Zhang, X. (2013a). The contribution of urbanization

508   to recent extreme heat events and a potential mitigation strategy in the

509   Beijing–Tianjin–Hebei metropolitan area. *Theoretical and Applied Climatology*,

510   1-10

511   Wang, M., Zhang, X., & Yan, X. (2013b). Modeling the climatic effects of

512   urbanization in the Beijing-Tianjin-Hebei metropolitan area. *Theoretical and*

513   *Applied Climatology, 113*, 377-385

514   Wang, X., Wu, Z., & Liang, G. (2009). WRF/CHEM modeling of impacts of

515   weather conditions modified by urban expansion on secondary organic aerosol

516   formation over Pearl River Delta. *Particuology, 7*, 384-391

517   Weng, Q. H. (2009). Thermal infrared remote sensing for urban climate and

518   environmental studies: Methods, applications, and trends. *Journal of*

519   *Photogrammetry and Remote Sensing, 64(4), 335-344.*

520   Weng, Q., Lu, D., & Liang, B. (2006). Urban surface biophysical descriptors and

521   land surface temperature variations. *Photogrammetric Engineering & Remote*

522   *Sensing, 72*, 1275-1286

523   Weng, Q.H., Lu, D.S., & Schubring, J. (2004). Estimation of land surface

524   temperature-vegetation abundance relationship for urban heat island studies.

525   *Remote Sensing of Environment, 89*, 467-483

526   Wu, R., Hu, Z.Z., Kirtman, B.P., 2003. Evolution of ENSO-related rainfall

527   anomalies inEast Asia and the processes. *Journal of Climate. 16, 3741-3757.*

528   Yang, B., Zhang, Y., & Qian, Y. (2012). Simulation of urban climate with

529   high-resolution WRF model: A case study in Nanjing, China. *Asia-Pacific*

530   *Journal of Atmospheric Sciences, 48*, 227-241

531   Yang, S. B.,Zhao, X. Y., Shen, S. H., Hai, Y.L., &Fang, Y. X. (2010).

532   Characteristics of urban heat island seasonal pattern in Beijing based on

533   LandsatTM/ETM+image. *Transactions of Atmospheric Sciences, 33(4),*

534   *427-435*

535   Zhang, C.L., Chen, F., Miao, S.G., Li, Q.C., Xia, X.A., & Xuan, C.Y. (2009).

536   Impacts of urban expansion and future green planting on summer precipitation

537   in the Beijing metropolitan area. *Journal of Geophysical Research:*

538   *Atmospheres, 114*, D02116

539   Zhang, G.H., Hou, Y.Y., Li,G.C., Yan, H., & Yang, L.M. (2005). Studies on the

540   diurnal and seasonal variations in the urban heat island and its factors in

541   Beijing city and its surrounding areas based on the remote sensing images.

542   *Science in China (Series D), 35, 187-194*

543   Zhang, H.,Qi, Z., Ye, X., Cai., Y., Ma, Y. &Chen., M. (2013). Analysis of land

544   use/land cover change, population shift, and their effects on spatiotemporal

545   patterns of urban heat islands in metropolitan Shanghai, China. *Applied*

546   *Geography, 44,* 121-133.

547   Zhang, N., Gao, Z., Wang, X., & Chen, Y. (2010). Modeling the impact of

548   urbanization on the local and regional climate in Yangtze River Delta, China.

549   *Theoretical and Applied Climatology, 102*, 331-342.